

Structural Evolution of Polyglycolide and Poly(glycolide-co-lactide) Fibers during In Vitro Degradation with Different Heat-Setting Temperatures

Yushuang Miao,^{||} Huashuai Cui,^{||} Zhimin Dong, Yi Ouyang, Yiguo Li, Qing Huang, and Zongbao Wang*



Cite This: *ACS Omega* 2021, 6, 29254–29266



Read Online

ACCESS |



Metrics & More

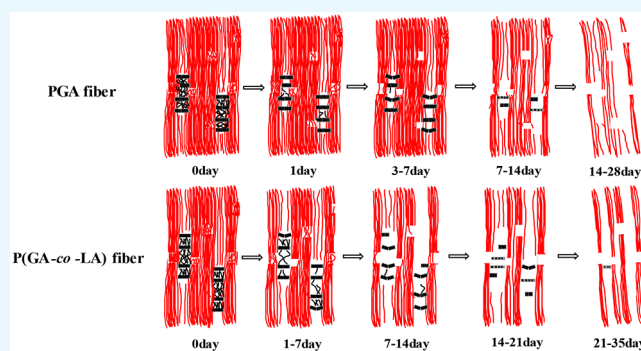


Article Recommendations



Supporting Information

ABSTRACT: The structural evolution of polyglycolide (PGA) and poly(glycolide-co-lactide) (P(GA-co-LA)) with 8% LA content fibers with different heat-setting temperatures was investigated during in vitro degradation using WAXD, SAXS, and mechanical property tests. It was found that the PGA fiber was more susceptible to the degradation process than the P(GA-co-LA) fiber and a higher heat-setting temperature reduced the degradation rate of the two samples. The weight and mechanical properties of the samples showed a gradual decrease during degradation. We proposed that the degradation of PGA and P(GA-co-LA) fibers proceeded in four stages. A continuous increase in crystallinity during the early stage of degradation and a gradual decline during the later period indicated that preferential hydrolytic degradation occurred in the amorphous regions, followed by a further degradation in the crystalline regions. The cleavage-induced crystallization occurred during the later stage of degradation, contributing to an appreciable decrease in the long period and lamellar thickness of both PGA and P(GA-co-LA) samples. The introduction of LA units into the PGA skeleton reduced the difference in the degradation rate between the crystalline and amorphous regions, and they were simultaneously degraded in the early stage of degradation, leading to a degradation mechanism different from that of the PGA fiber.



1. INTRODUCTION

Biodegradable polymer materials are an important class of synthetic biomaterials, which are widely used in medical fields such as wound healing and tissue regeneration. Most of these polymers have biodegradable skeletons and are composed of esters, anhydrides, carbonates, and so on.^{1–4} Among the developed biodegradable polymers, aliphatic polyesters have attracted much attention due to their good melt processability, mechanical strength, and excellent degradability. Polyglycolide (PGA), Polylactide (PLA), and their copolymers Poly(glycolide-co-lactide) (P(GA-co-LA)) are typical examples of aliphatic polyesters, which are of good properties for biomedical applications mainly in degradable and absorbable sutures, and drug release systems.^{5–13} PGA fibers have good biocompatibility but with high Young's modulus, poor flexibility, and fast strength degradation, whereas PLA fibers have a long degradation period. Therefore, to better meet the requirements of surgical sutures, scientists adopted the copolymerization method to introduce the LA segment with excellent biodegradability and biocompatibility into the PGA segment to synthesize P(GA-co-LA).^{14–16} The P(GA-co-LA) fibers, of which GA is the main component, have been developed into surgical sutures owing to their excellent tensile strength and appropriate degradation rate in vitro as well as

other mechanical and biological properties. A commercial product having a proven record in clinical applications is VICRYL[®] (Ethicon trademark) Suture, which is based on one of the P(GA-co-LA) copolymers and has been widely used.

To ensure the high quality and safety of sutures during use, two important properties must be satisfied.^{17,18} One is the mechanical properties, especially the tensile strength of sutures, which determines the ability of wound tissue to bind; the other is degradation performance, which mainly relates to the retention of breaking strength. Therefore, it is of great importance to study the degradation characteristics of polymer sutures. At present, many investigations have been carried out to understand the degradation behavior of these polymers during in vitro and in vivo biochemical applications.^{19–31} For example, Chu et al.^{25,26} studied the effect of buffer solution on the degradation of PGA sutures and concluded the importance of crystallinity on tensile strength. They proposed that the

Received: September 8, 2021

Accepted: October 5, 2021

Published: October 19, 2021



degradation was carried out in two different stages, each with a different degradation rate, which is closely related to the amorphous and crystalline regions in the samples. Fredericks et al.^{27,28} showed that the hydrolysis process was composed of two main mechanisms. Water molecules first diffused into the amorphous region since this area was less organized and more accessible by water molecules, leading to the scission of some disordered chains, and “cleavage-induced crystallization” occurred due to the scission of amorphous chains with the significant increase in mobility; as a result, the crystallinity would reach the maximum. Then, water molecules could slowly attack the crystalline phase, resulting in the chain segments small enough to dissolve in water and be easily metabolized.²⁹ Li³⁰ investigated the detailed degradation mechanism and the effects of various factors on the degradation of P(GA-co-LA) polymers and found that the internal degradation rate was faster than that of the surface as a result of the larger autocatalytic effect. Zong et al.³¹ investigated the changes of the crystal structure and morphology in PGA and P(GA-co-LA) during in vitro degradation and found that the mass degree of crystallinity showed an Avrami-like behavior in both samples and the long period and lamellar thickness decreased appreciably owing to the cleavage-induced crystallization process. In summary, scientists have done much research about the degradation of PGA and P(GA-co-LA) in the past time. However, the degradation mechanism has not been thoroughly studied, especially regarding the relationship between the degradation and the preparation process, which limits our capability to modulate the degradation performance of the final product.

As we all know, the performance of polymer fibers depends largely on their aggregation structure, which varies with processing technology. Currently, two typical processing techniques are mainly used to manipulate the properties of fibers.¹⁸ One involves the hot-stretching process and the other involves the heat-setting process. As a typical aliphatic polyester, the degradation performance of PGA and P(GA-co-LA) fibers is decisively affected by their aggregation structure. Therefore, it is of great significance to establish the relationship between the aggregation structure and degradation properties, particularly for the PGA and P(GA-co-LA) fibers with the different hot-stretching and heat-setting conditions, which has a guiding significance to modulate the mechanical properties and degradation properties of PGA and P(GA-co-LA) fibers, as well as to develop high-performance absorbable sutures.

Our group systematically studied the structural evolution of PGA and P(GA-co-LA) fibers during the heat-setting process recently.³² In this study, on the basis of the previous work, the degradation performance of PGA and P(GA-co-LA) fibers at different heat-setting temperatures during degradation was deeply studied by WAXD, SAXS, and DSC measurements, as well as mechanical property tests and the possible degradation mechanism was also provided.

2. EXPERIMENTAL SECTION

2.1. Material. The PGA raw material with an intrinsic viscosity of 1.6 dL/g was purchased from Purac company of the Netherlands, and the P(GA-co-LA) raw material with an intrinsic viscosity of 1.55 dL/g was purchased from Chengdu Yihe Hengrui Medical Technology Co., Ltd., in which the molar content of LA was 8%. PGA and P(GA-co-LA) raw materials were added into the screw extruder and extruded at

250 °C for spinning. The fibers were made by winding with a drafting roller and a setting roller with a drafting temperature of 60 °C and a drawing ratio of 4.5. The fibers were then subjected to hot-stretching and kept in a vacuum glove box. The PGA and P(GA-co-LA) fibers were placed in a vacuum drying oven for annealing treatment, the annealing temperature was 100, 120, and 140 °C, respectively, and the annealing time was 2 h, then the annealed fiber samples were obtained.

2.2. In Vitro Degradation. The phosphate buffer (Sigma Scientific) was mixed with deionized water in a ratio of 1:10 to produce a phosphate buffer solution (PBS) with a pH of 7.40. Several clean beakers were taken and an equal amount of phosphate buffer solution was poured into them; the weighed original fiber samples and the annealed samples were added to the beakers and then placed in a water-proof incubator at 37 °C for an in vitro degradation study. During the degradation process, the whole degradation system remains static. The pH value of the PBS was closely monitored during the experiments. To ensure that the experimental process can smoothly simulate the steady-state conditions of the human body, the phosphate buffer solution was replaced every two days to guarantee that the pH value can be maintained at about 7.40. It should be noted that we also conducted a separate set of experiments in which a single fiber sample of approximately the same mass was placed in a beaker containing an equal amount of PBS and did not change the solution during the degradation period to measure the pH value, and the result was displayed in Figure S1 in the Supporting Information. Within a certain time interval, the fiber samples were taken from the solution and gently washed three times in distilled water, absorbed the surface moisture with filter paper, dried in a vacuum drying oven for 24 h, and then proceeded with subsequent tests. The weight changes of these samples were examined as a function of degradation time. According to the following eq 1, the mass loss (W_1) was calculated by comparing the dried weight (W_d) remaining at a given degradation time with the initial weight (W_0)

$$W_1\% = 100 \times (W_0 - W_d) / W_0 \quad (1)$$

2.3. Mechanical Property Test. The mechanical property test was performed using the Linkam TST350 tensile machine with a stretching rate of 10 mm/min. The tensile strength and strain of the samples in different degradation days were obtained from the tensile test, and at least five samples were used for each data point, and their average values were taken.

2.4. DSC Measurements. DSC measurements were performed with Pekin Elmer DSC8000 under a nitrogen atmosphere. About 6 mg of degraded samples were heated at a rate of 10 °C/min from room temperature to 250 °C. The ΔH can be obtained by extrapolating the post-melting baseline.

2.5. WAXD and SAXS Measurements. The offline WAXD and SAXS measurements were carried out at the BL16B1 beamline in the Shanghai Synchrotron Radiation Facility (SSRF). The prepared fibers with different degradation days were pasted on the sample table for testing. The X-ray wavelength was 0.1239 nm. The sample-to-detector distance was 268 mm for WAXD and 2003 mm for SAXS, and the image acquisition time for each data of both WAXD and SAXS was 20 s. Two-dimensional (2D) WAXD and SAXS patterns were recorded with a Pilatus 1 M and Pilatus 2 M, respectively. All X-ray images were corrected for background scattering, air scattering, and beam fluctuations.

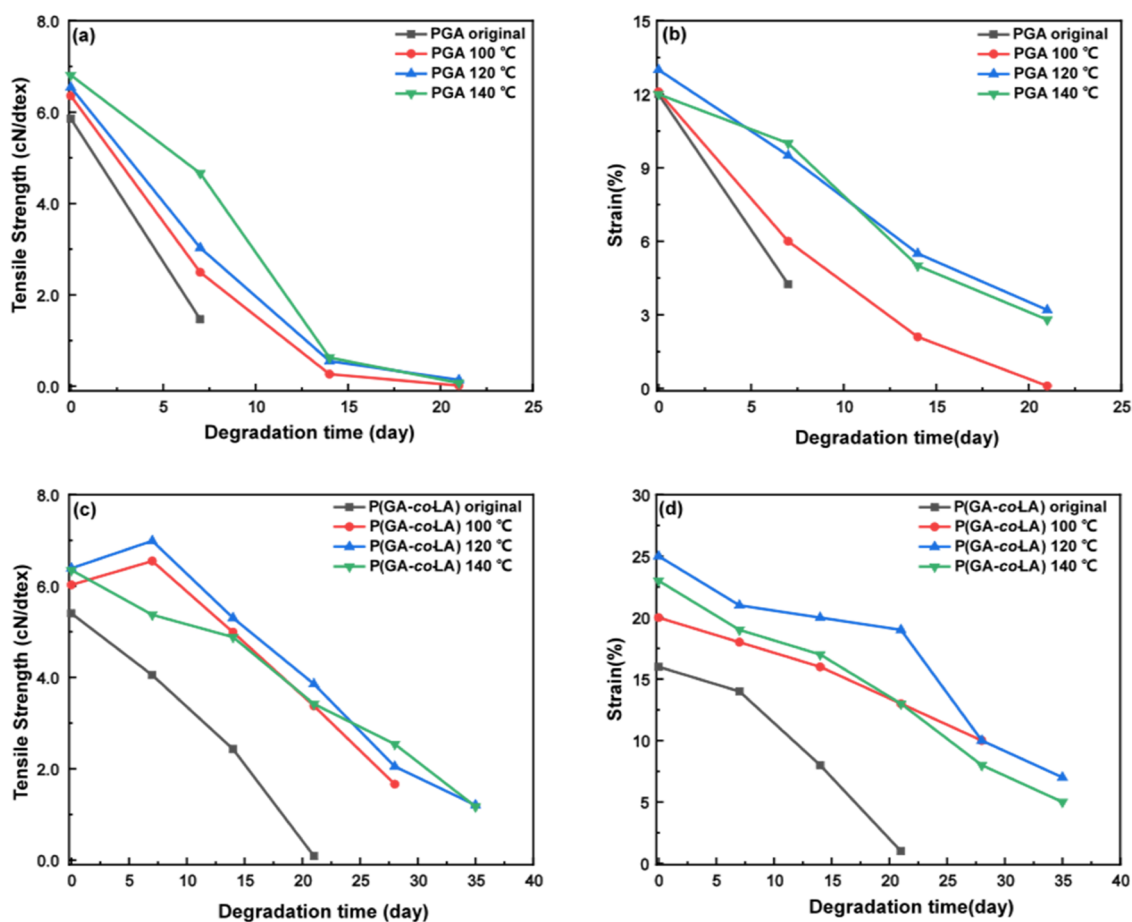


Figure 1. The tensile strength (a and c) and strain (b and d) of PGA and P(GA-co-LA) fibers during in vitro degradation with different heat-setting temperatures. At least five samples were used to test the stretch curves.

2.6. WAXD and SAXS Data Analysis. The analyses of WAXD data were processed by pyFAI software, and the SAXS data was carried out using the Fit2d software package,³³ and partial data was evaluated using ipyChord.³⁴ In WAXD analysis, the degree of crystal orientation was obtained using Herman's method.³⁵ In specific, the degree of orientation, f_{020} , was calculated from the azimuthal intensity distribution of the (020) crystal reflection. The crystallinity was calculated according to the diffraction intensity of the crystalline phase and the amorphous phase.

The orthorhombic unit cell parameters a and b were evaluated in terms of the following equation using the crystalline plane analysis

$$\frac{1}{d_{hkl}^2} = \frac{h^2}{a^2} + \frac{k^2}{b^2} + \frac{l^2}{c^2} \quad (2)$$

where h , k , and l are the Miller indices and d_{hkl} is the interplanar spacing, defined by Bragg's law

$$d_{hkl} = \frac{\lambda}{2 \sin \theta} \quad (3)$$

where λ is the X-ray wavelength and θ is the diffraction angle.

The (110) and (020) reflection peaks were used to determine the crystallite sizes. This measurement was performed using the Scherrer equation

$$D_{hkl} = \frac{K\lambda}{\beta \cos \theta} \quad (4)$$

where K is the shape factor ($=0.89$), λ is the wavelength (0.1239 nm), and β is the experimental breadth at the maximum intensity.

SAXS is a method that can detect long period and lamellar thickness, whose patterns reflect the long period ($L = L_a + L_c$) of the crystalline phase (L_c) and the amorphous phase (L_a) stacking. In our study, the one-dimensional electron density correlation function $K(z)$ provides a practical approach to quantify the lamellar and amorphous thickness.^{36–38} $K(z)$ can be defined as

$$K(Z) = \frac{\int_0^\infty i(s)s^2 \cos(2\Pi s z) ds}{\int_0^\infty i(s)s^2 ds} \quad (5)$$

where s is the reciprocal space coordinate, defined as $s = 2 \sin \theta / \lambda$.

3. RESULTS AND DISCUSSION

3.1. Changes of Mechanical Properties during Degradation. It is well known that surgical sutures must meet certain mechanical properties during the degradation process to ensure the safety and stability of clinical use. Therefore, it is of great importance to study the changes in the mechanical properties of fibers during the degradation process. Figure 1 illustrates the changes of the mechanical properties of the PGA and P(GA-co-LA) fibers during degradation with different heat-setting temperatures. With the degradation, the mechanical properties showed a significant decrease, and the

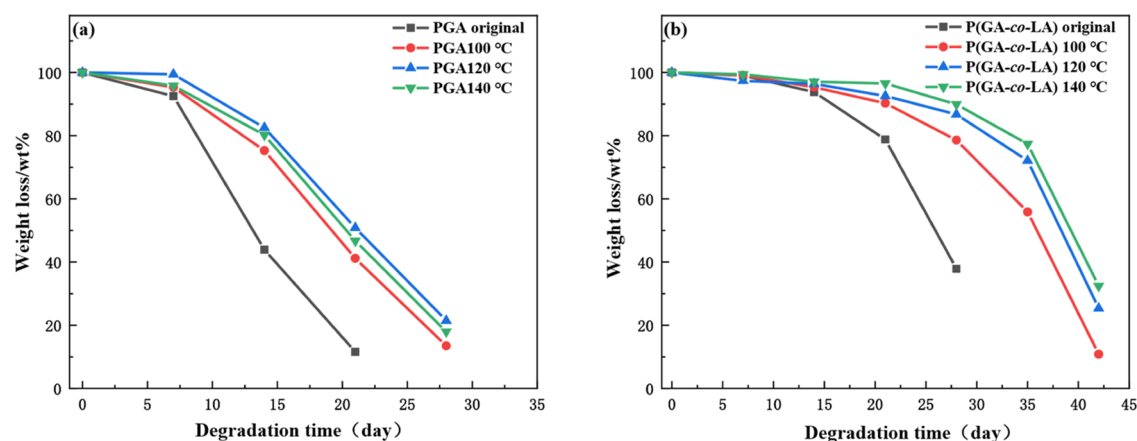
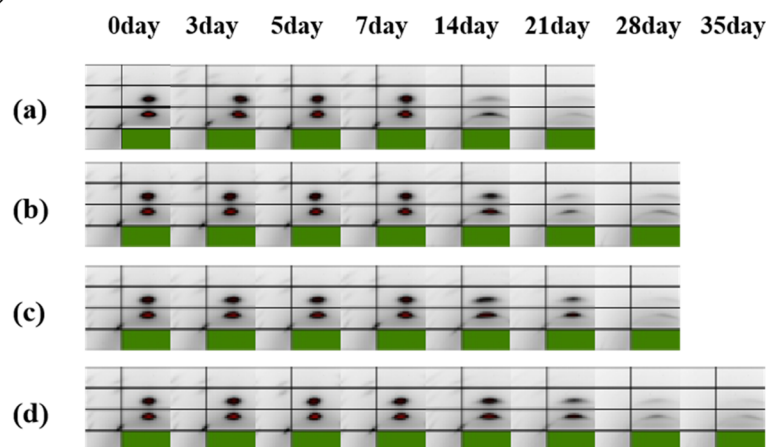


Figure 2. Weight loss of (a) PGA and (b) P(GA-co-LA) fibers during in vitro degradation with different heat-setting temperatures.

(A) PGA



(B) P(GA-co-LA)

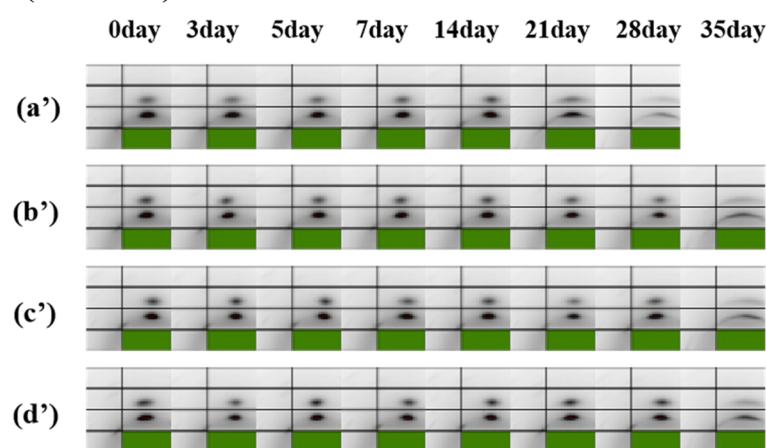


Figure 3. 2D WAXD patterns of (A) PGA and (B) P(GA-co-LA) fibers with different heat-setting temperatures at different degradation days. (a) PGA original, (b) PGA 100 °C, (c) PGA 120 °C, (d) PGA 140 °C, (a') P(GA-co-LA) original, (b') P(GA-co-LA) 100 °C, (c') P(GA-co-LA) 120 °C, and (d') P(GA-co-LA) 140 °C.

samples after heat-setting were obviously more resistant to degradation. Basically, the mechanical properties of samples decreased at a slower rate during degradation with the increase of heat-setting temperatures. However, it must be mentioned that the heterogeneity of the degraded fiber samples would lead to less consistent regularity. The PGA original fibers lost their tensile strength after 7 days of degradation, while the

samples after heat-setting were maintained for nearly 14 days. However, the P(GA-co-LA) original fibers basically lost their tensile strength after 21 days of degradation, while the tensile strength of the samples after heat-setting can be maintained for about 35 days. The initial reduction in strength was considered to be mainly due to the rapid degradation of the amorphous phase.³⁹ These results illustrated to some extent that the

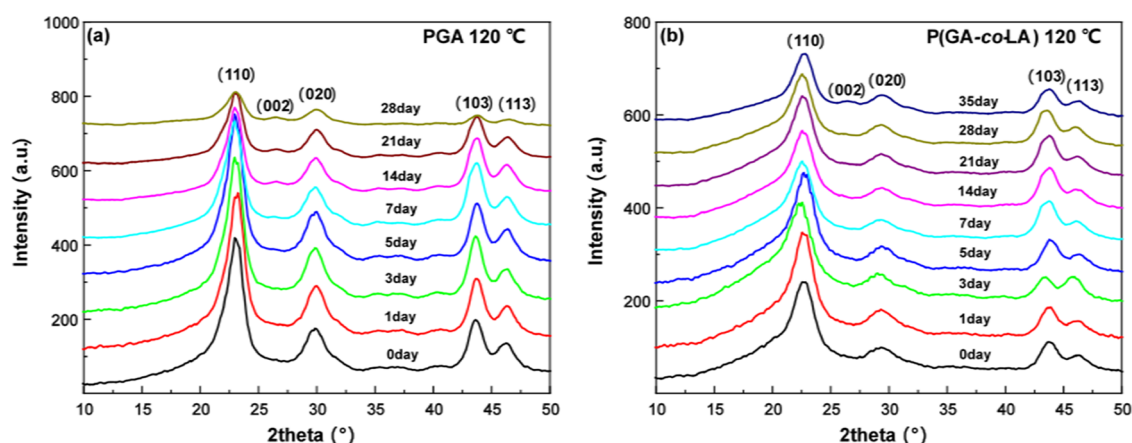


Figure 4. 1D WAXD curves of (a) PGA and (b) P(GA-co-LA) fibers with the heat-setting temperature of 120 °C during in vitro degradation.

introduction of LA unit segments into PGA was conducive for delaying the degradation rate and maintaining the mechanical properties during the degradation process.

3.2. Weight Changes during Degradation. The degradation of aliphatic polyesters occurs through simple hydrolysis of the ester backbone under aqueous conditions.^{40,41} The degradation rate depends on the molecular weight, crystallinity, orientation, morphology, and so on. Data in Figure 2 shows the weight loss of PGA and P(GA-co-LA) fibers during degradation with different heat-setting temperatures. Obviously, as the degradation process goes on, both the PGA and P(GA-co-LA) fibers lose weight gradually. The degradation rate of the samples after heat-setting was slower than that of the samples without heat-setting, and different heat-setting temperatures had little impact on the weight loss of the PGA samples, whereas the P(GA-co-LA) samples were more resistant to degradation with the increase of heat-setting temperatures. The PGA fibers exhibited a very slow rate of weight loss during the first 7 days of degradation, after which weight loss began to accelerate. The residual weight of the original PGA fibers was only 10% after 21 days of degradation, while the PGA fibers after heat-setting were more than 40% after 21 days of degradation and about 15% after 28 days of degradation. In addition, no weight loss data were available since the PGA samples became too fragile to be collected. On the contrary, the P(GA-co-LA) fibers showed a slower degradation rate compared with the PGA fibers. The residual weight of the original P(GA-co-LA) fibers was less than 40% after 28 days of degradation, whereas the weight of the P(GA-co-LA) fibers after heat-setting retained approximately 80% after 28 days of degradation and 20% after 42 days of degradation. The higher weight loss of PGA as compared to P(GA-co-LA) can be attributed to the difference in the degradation rate. Since the introduction of the methyl group of the side chain in P(GA-co-LA) improved the hydrophobicity, and the methyl group connected to the ester group also increased the steric hindrance of the nucleophilic group to attack the C–O bond in the ester group, thus reducing the degradation rate. According to the literature, the hydrolytic degradation process could also be divided into two stages. In the first stage, almost no weight loss occurred, but the molecular weight of the samples decreased continuously as the degradation time increased. As the hydrolytic time increased, the molecular weight of the samples decreased to a low value and remained relatively constant with further degradation,

while the samples experienced a significant weight loss.^{42,43} Therefore, at the initial stage of degradation of PGA and P(GA-co-LA) fibers, although the ester bond was broken, some molecules were not small enough to be soluble in water, resulting in a small weight loss. The acceleration of weight loss can be assigned to the fact that more and more soluble oligomers were formed and released.

3.3. WAXD and SAXS Results. To understand the changes in these properties of PGA and P(GA-co-LA) fibers during the degradation process preferably, it was necessary to combine them with the structure. The selected 2D WAXD patterns of PGA and P(GA-co-LA) fibers with the different heat-setting temperatures at different degradation days are presented in Figure 3. It can be found that the WAXD patterns of PGA and P(GA-co-LA) fibers composed of two diffraction spots corresponding to (110) and (020) crystalline planes of orthorhombic form, respectively, which indicated that the structure of PGA and P(GA-co-LA) fibers have a high orientation. As can be seen from the 2D WAXD patterns, the diffraction signals of (110) and (020) crystalline planes became significantly weaker with degradation, and the signals gradually transformed from spots to arcs, indicating the decrease of orientation in the process of degradation. The signal of the unannealed PGA samples showed an obvious decrease after 7 days of degradation, whereas the signal of the annealed samples showed obvious change after 21 days or even 28 days of degradation, indicating that the samples after heat-setting possessed a fair resistance to degradation and showed a slower rate of degradation with the increase of the heat-setting temperatures. Compared with PGA, the P(GA-co-LA) fibers caused a slower decrease in intensity because of the slower degradation rate.

Figure 4 illustrates the representative 1D WAXD curves extracted from the 2D WAXD patterns during in vitro degradation of PGA and P(GA-co-LA) fibers at the heat-setting temperature of 120 °C (similar data were obtained for PGA and P(GA-co-LA) fibers at 100 and 140 °C, as depicted in Figure S2 in the Supporting Information, and, therefore, the discussion was valid for all samples). Two main diffraction peaks corresponding to the two bright spots in 2D WAXD patterns can be seen in both PGA and P(GA-co-LA) samples during degradation. The diffraction peak of $2\theta = 22.9^\circ$ corresponded to the (110) crystalline plane, while the diffraction peak of $2\theta = 29.7^\circ$ corresponded to the (020) crystalline plane. In addition to the two strong crystalline

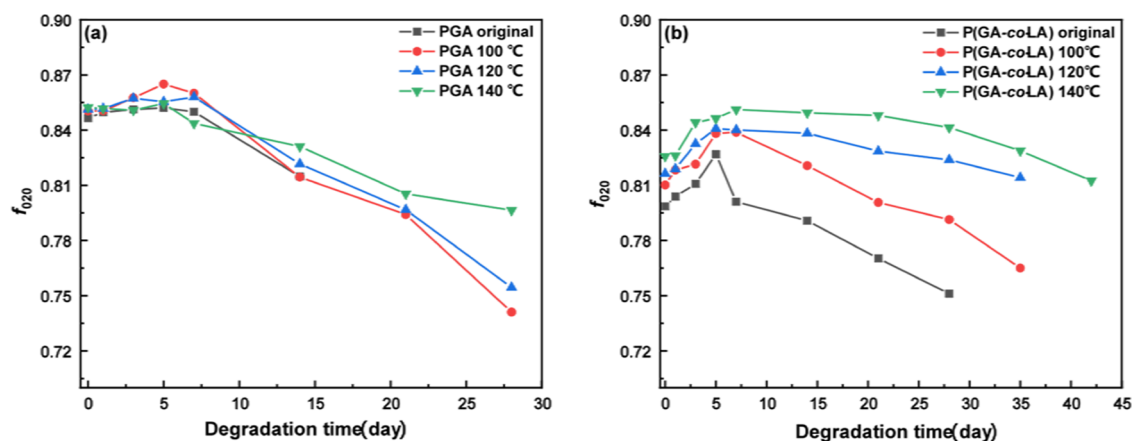


Figure 5. Degree of crystal orientation for (a) PGA and (b) P(GA-co-LA) fibers with different heat-setting temperatures during in vitro degradation.

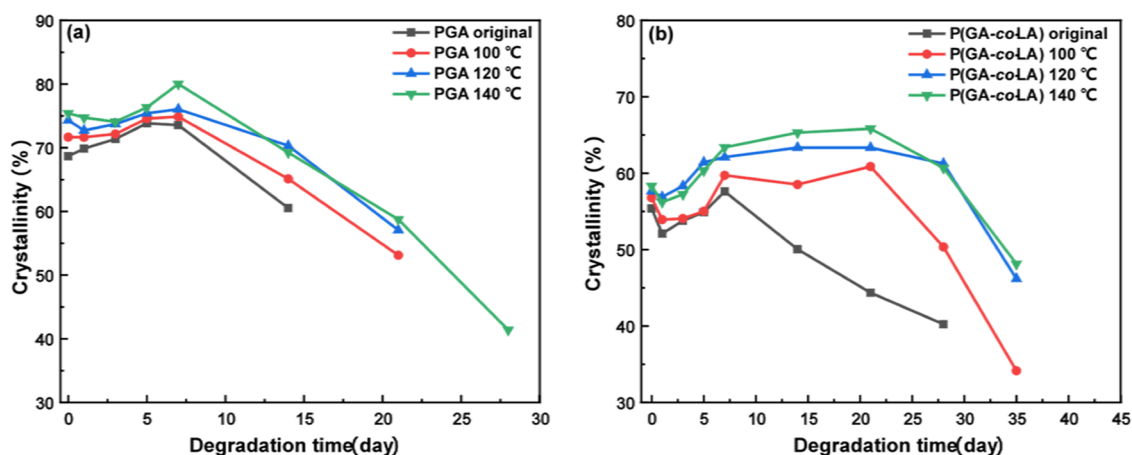


Figure 6. Crystallinity for (a) PGA and (b) P(GA-co-LA) fibers with different heat-setting temperatures during in vitro degradation.

planes, other reflection peaks, located at 26.2, 43.6, and 46.2°, were also observed, corresponding to (002), (103), and (113) crystalline planes, respectively, which were assigned on the basis of the orthorhombic unit cell structure of both PGA and P(GA-co-LA) samples. It can be drawn from the figure that the diffraction peak intensity of the fibers increased first and then decreased with the degradation. From the changes of diffraction peak intensity, it was obvious that the P(GA-co-LA) fibers were more resistant to degradation than the PGA fibers. Besides, the appearance of the (002) crystalline plane indicated that the framework of the fibrillar crystal collapsed and the crystal inclined during the degradation. Certainly, we had also verified whether the appearance of the (002) crystalline plane was caused by the existence of the fiber itself or by degradation, and the results are presented in Figure S3 in the Supporting Information, which indicated that the appearance of the (002) crystalline plane was indeed caused by collapsed fibrillar crystal during degradation.

The degree of crystal orientation calculated from WAXD results based on Herman's method for all heat-setting temperatures is shown in Figure 5. It can be observed that the degree of crystal orientation of PGA fibers was larger than that of P(GA-co-LA) fibers at the initial stage, which was in line with our expectation since the introduction of a part of LA units into GA unit segments would destroy the integrity of crystal. Compared with PGA, the P(GA-co-LA) samples caused a slower decrease in orientation because of the slower

degradation rate. Moreover, the decreasing tendency of the orientation degree would obviously be reduced with the heat-setting temperature. The change of orientation can be roughly divided into two stages. In the first stage, the orientation showed a slight increase, which was considered to be related to the different degradation rates of lamellar and fibrillar crystals. After that, the orientation showed a gradual decrease, which is probably due to the degradation of some crystalline regions and collapsed fibrillar crystals.

The changes in the crystallinity of PGA and P(GA-co-LA) samples during degradation in PBS are shown in Figure 6. The crystallinity change trend obtained from the DSC results was consistent with it, as displayed in Figure S4 in the Supporting Information. It should be emphasized that during the heat-setting process, the polymer chains gained mobility as a result of the elevated temperature; consequently, some disordered molecular chains tend to crystallize, resulting in an increase of the initial crystallinity of degradation with the heat-setting temperature. A slight increase in the crystallinity for PGA samples was observed within the first 7 days of degradation, and thereafter the crystallinity gradually decreased until the later stage. However, for P(GA-co-LA), the crystallinity gradually increased until about 21 days during degradation and subsequently decreased. This was also corresponding to the previous decrease in mechanical properties. An increase in crystallinity during hydrolytic degradation had been previously observed in both PGA and P(GA-co-LA) samples.^{44–46}

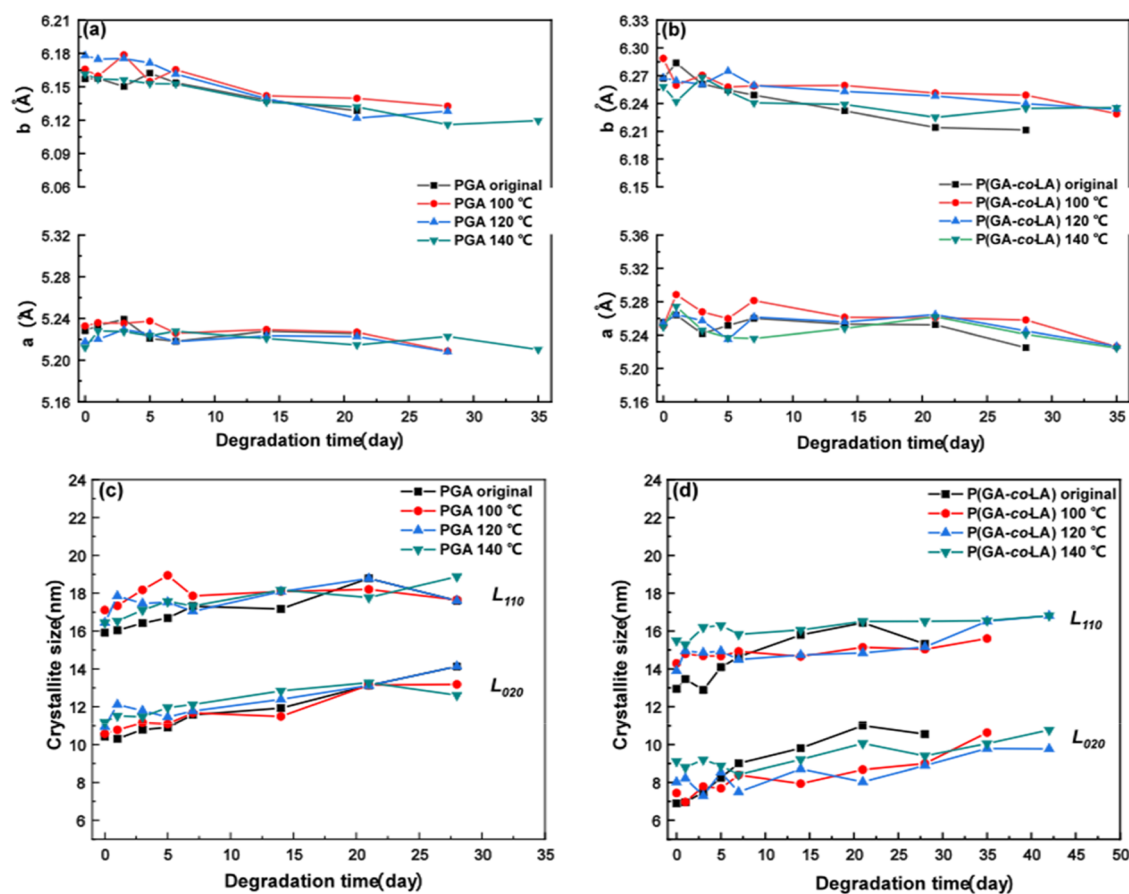


Figure 7. Unit cell parameters (a and b) and lateral crystallite sizes (c and d) by the crystalline planes of (110) and (020) of PGA and P(GA-co-LA) fibers with different heat-setting temperatures during in vitro degradation.

Although the increase in crystallinity was not large, it was of great significance because very little weight was lost during the first 7 days of degradation for PGA fibers, which indicated that the preferential hydrolytic degradation occurred in the amorphous regions in the early stage of degradation. The increase of crystallinity can also be explained by cleavage-induced crystallization to some extent, as the tie chains in the amorphous regions can degrade into fragments, resulting in a lower degree of entanglement by the long-chain molecules in the amorphous regions.^{31,47} However, it should be pointed out that the degradation environment was conducive to the crystallization of short-chain molecules, which may also be one of the reasons. After that, the crystallinity decreased at the later stage of degradation, illustrating that the degradation of some crystalline regions occurred. Similar results were obtained for P(GA-co-LA) fibers and, therefore, the discussion was valid for both samples. However, we have only given a general explanation of crystallinity; the detailed reasons for the trend of crystallinity will be discussed later. The cleavage-induced crystallization behavior will also be elaborated through the addition SAXS experiment in the next section.

The positions of the two reflection peaks (110) and (020) were used to calculate the unit cell parameters a and b and lateral crystallite sizes L_{110} and L_{020} . All changes in structural parameters (orthorhombic unit cell parameters a and b ; lateral crystallite sizes, L_{110} and L_{020}), extracted from the WAXD data, are summarized in Figure 7. It was seen that both unit cell parameters (a and b) exhibited a slight decrease during degradation. It was, however, interesting to see that the unit

cell parameter b decreased at a faster rate than unit cell parameter a , which was related to the existence of weak hydrogen bonds on the (110) crystalline plane of PGA.⁴⁸ The effect of heat-setting temperatures on the unit cell parameters during degradation was small, and the decrease of the unit cell parameters reflected the overall increase in crystal perfection, probably accomplished by the removal of constraints on the crystal surfaces since the larger unit cells on the surface were preferentially degraded. It was worth noting that the value of unit cell parameters of P(GA-co-LA) was higher than PGA, which suggested that LA was indeed discharged into the GA unit segments, forming a eutectic. In addition, the corresponding lateral crystallite sizes L_{110} and L_{020} showed a gradual increase during degradation because smaller crystals were fully lost more readily due to their large specific surface area, thereby increasing the average crystallite sizes. This result may alternatively be interpreted as an increase in crystal perfection achieved as constraints were removed by the degradation of the amorphous material.⁴⁴ However, the cleavage-induced crystallization was also one of the key reasons for the increase of crystallite sizes. It can also be observed from Figure 7c and d that the crystallite sizes of PGA fibers were larger than that of P(GA-co-LA) fibers at the initial stage. Actually, the spacing between the PGA atomic lattice layers increased with the introduction of the LA units, and the LA units loosened the crystal packing and decreased the crystallite sizes, resulting in the crystallite sizes of the P(GA-co-LA) fibers that had a lower value than PGA fibers at the initial stage.

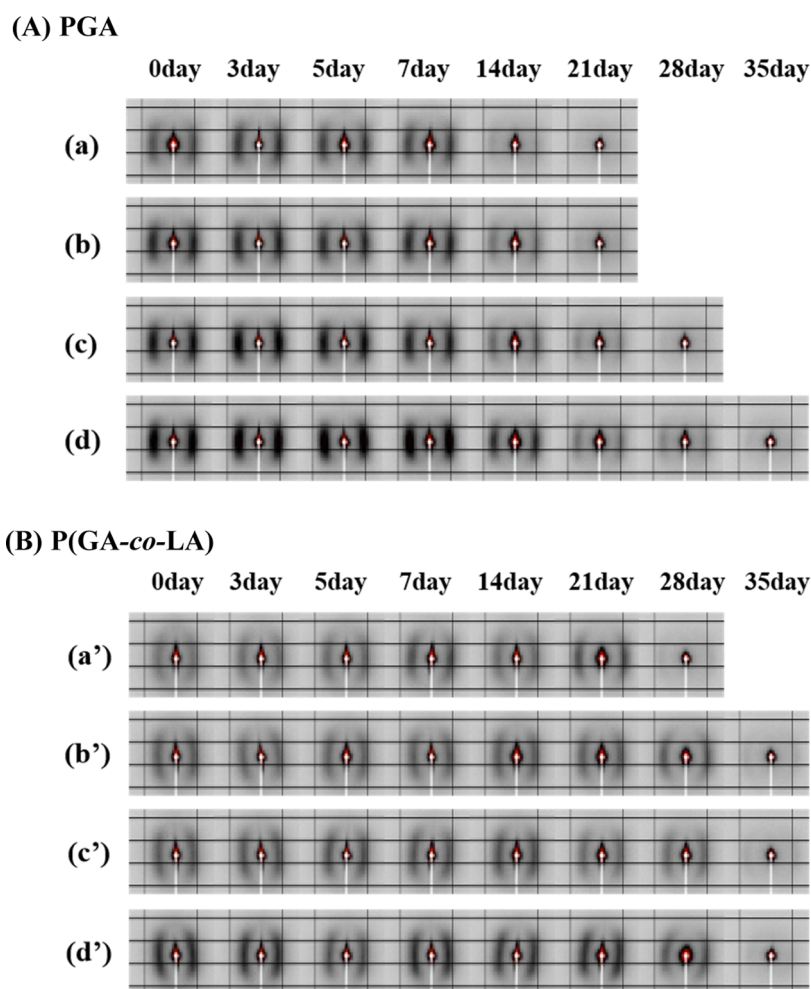


Figure 8. 2D SAXS patterns of (A) PGA and (B) P(GA-co-LA) fibers with different heat-setting temperatures at different degradation days. (a) PGA original, (b) PGA 100 °C, (c) PGA 120 °C, (d) PGA 140 °C, (a') P(GA-co-LA) original, (b') P(GA-co-LA) 100 °C, (c') P(GA-co-LA) 120 °C, and (d') P(GA-co-LA) 140 °C.

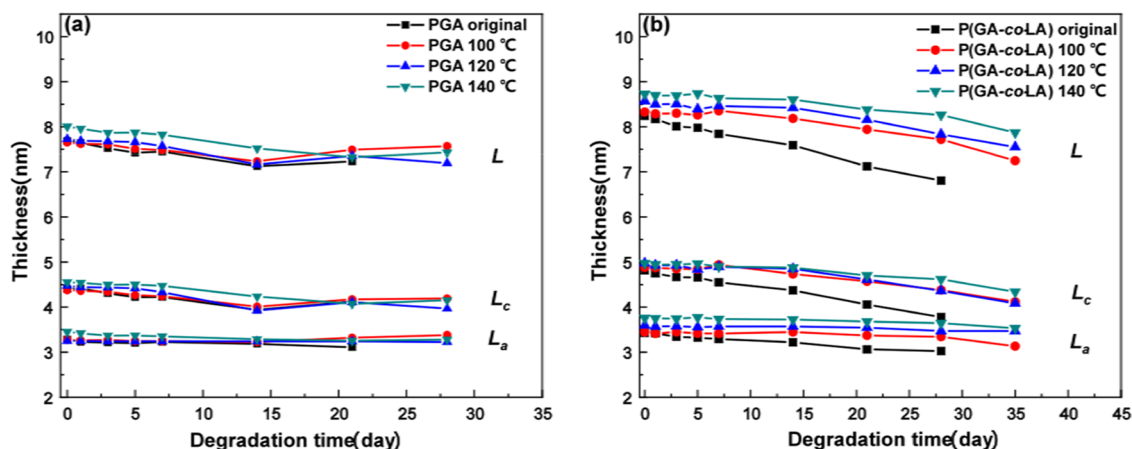


Figure 9. Structural parameters (L , L_c , and L_a) as a function of the degradation time calculated by one-dimensional electron density correlation function of (a) PGA and (b) P(GA-co-LA) fibers with different heat-setting temperatures.

Figure 8 shows the selected 2D SAXS patterns of PGA and P(GA-co-LA) fibers with different heat-setting temperatures at different degradation days. It can be seen that the scattering pattern of PGA and P(GA-co-LA) fibers consisted of a longitudinal streak and two other scattering patterns. The longitudinal streak across the beam stop was corresponded to

the signal of the fibrillar crystals, whereas the two scattering patterns along the horizontal direction on both sides of the beam stop corresponded to the signal of the lamellar crystals. The scattering pattern of both fibrillar crystals and lamellar crystals gradually weakened with degradation; certainly, the intensity of the lamellar crystals decreased at a faster rate than

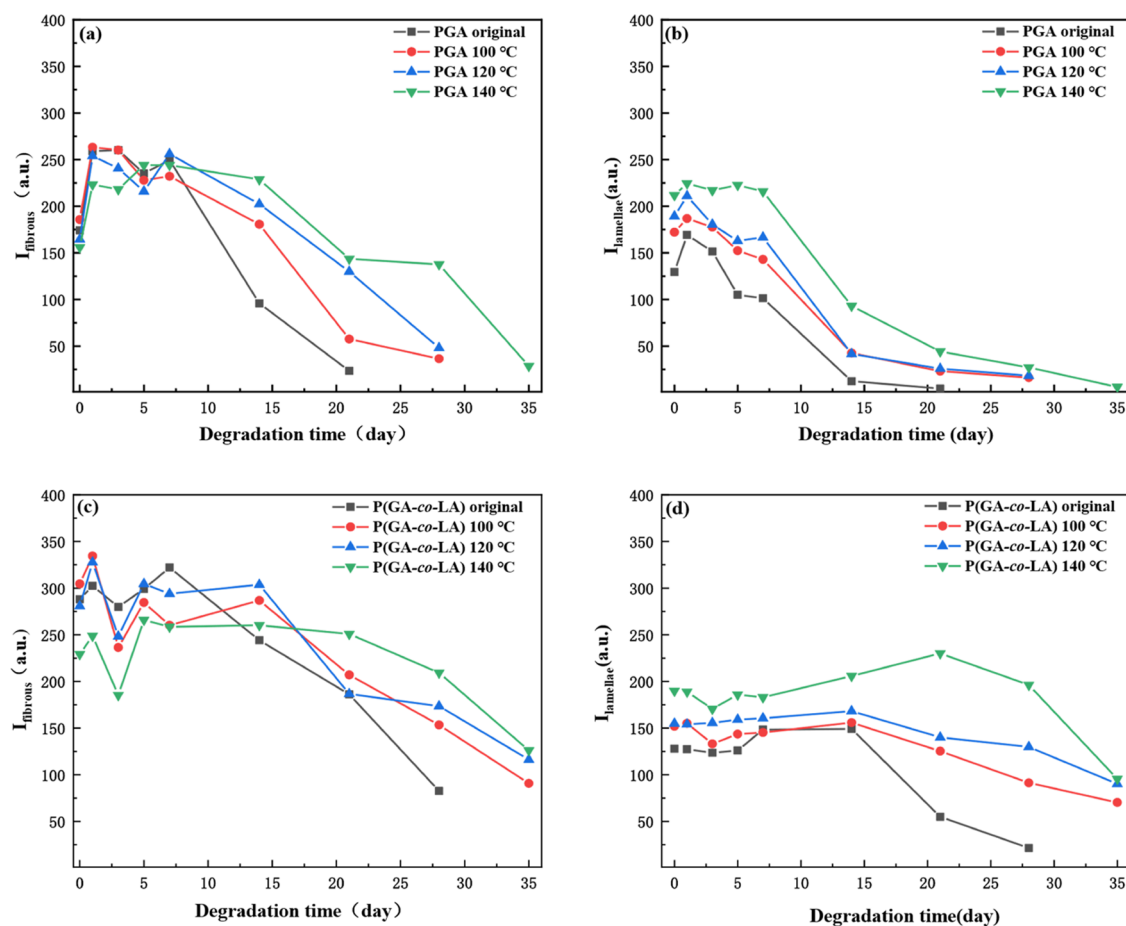


Figure 10. Scattering intensity of fibrillar (a and c) and lamellar crystals (b and d) of PGA and P(GA-co-LA) fibers with different heat-setting temperatures during degradation.

fibrillar crystals, which indicated that the degradation rate of the lamellar crystals was obviously faster than the fibrillar crystals. Moreover, the fiber resistance to degradation increased as the heat-setting temperature increased. The lamellar signal of PGA basically disappeared after 21 days, whereas the lamellar signal of P(GA-co-LA) was still obvious after 35 days of degradation, which also indicated that P(GA-co-LA) was more resistant to degradation than PGA fibers.

The one-dimensional SAXS profiles, extracted from the 2D SAXS patterns (as depicted in Figure S5 in the Supporting Information), were analyzed via the method of correlation function to estimate the lamellar structural variables of PGA and P(GA-co-LA) structures during degradation. The structural variables, including the long period L , the lamellar thickness L_c , and the amorphous layer thickness L_a , were calculated, as presented in Figure 9. The values of L and L_c of PGA samples were found to decrease slightly during the first 7 days and then showed a marked decline in 7–14 days, and ultimately remained nearly constant during the subsequent period. The amorphous layer thickness L_a basically remained unchanged or slightly reduced during degradation. The changing trend of P(GA-co-LA) was similar to that of PGA, except that the obvious decline of L and L_c occurred after 14 days during degradation. It was seen that the values of L , L_c , and L_a of P(GA-co-LA) after heat-setting were higher than PGA at the initial stage, which probably can be attributed to the lower degree of supercooling in P(GA-co-LA) fiber at the chosen heat-setting temperature.³¹ However, P(GA-co-LA)

without heat-setting was also larger than PGA, indicating that in addition to the degree of supercooling, it was also related to the lamellar structure between them since LA units were partially discharged into the GA structure to form a sandwich structure, resulting in a corresponding increase in the long period. Furthermore, it was also interesting to find out that the effect of heat-setting on P(GA-co-LA) was obvious but not on PGA. The values of L , L_c , and L_a increased with the heat-setting temperature. The marked decline of the long period and lamellar thickness was related to cleavage-induced crystallization. It was believed that the secondary crystallization can form thinner crystallites in the amorphous gaps and result in a dual population of lamellar stacks, which has been elaborated in many crystalline polymers,^{49–51} including PGA and P(GA-co-LA). As the water molecules penetrated into the amorphous region, causing the scission of disorder chains, it increased the chain mobility and facilitated the crystallization process in the amorphous regions, and this was similar to the secondary crystallization process. However, owing to the confined spatial restrictions and lower molecular mass species in the amorphous regions, the resultant lamellar thickness by cleavage-induced crystallization was thinner, which caused the averaged long period and lamellar thickness to decrease,⁵¹ as seen in Figure 9.

To further analyze the degradation stage of fibrillar and lamellar crystals, the relative scattering intensity of fibrillar and lamellar crystals during degradation is displayed in Figure 10. It was believed that when the degradation first occurred in the

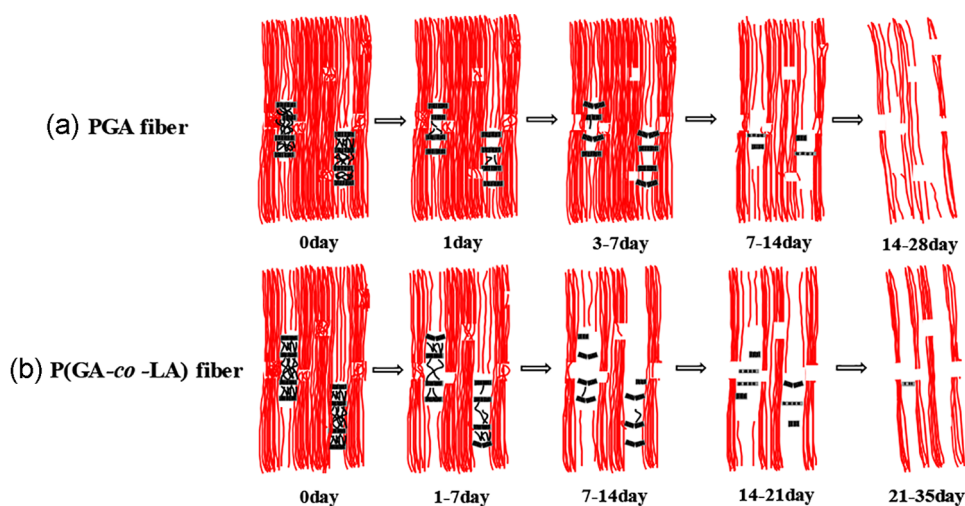


Figure 11. Schematic diagram of a four-stage model of the in vitro degradation mechanism of the original (a) PGA (b) P(GA-co-LA) fiber samples. Stages I and II, the amorphous regions of fibrillar and lamellar crystals were degraded, while the crystalline regions were partially degraded, the mechanical properties were decreased, but very little mass of the PGA and P(GA-co-LA) samples was lost. Stage III, the mobility of polymer chains within amorphous gaps increased after chain scission, cleavage-induced crystallization occurred. Stage IV, most of the fibrillar and lamellar crystals were degraded, and the fibers began to break down.

amorphous region, the difference of electron density will increase, resulting in the increase of the relative scattering intensity. Therefore, the increase of the scattering intensity in the initial stage of degradation mainly corresponded to the degradation of the amorphous regions, whereas the decrease in the subsequent stage corresponded to the degradation of crystalline regions. For PGA, the amorphous regions of the fibrillar crystals degraded in the first 7 days, and then the crystalline regions of the fibrillar crystal degraded. On the other hand, the amorphous regions of the lamellar crystals were degraded on the first day, and then the crystalline regions of the lamellae were degraded. Different from PGA, the degradation rates of P(GA-co-LA) in crystalline and amorphous regions were not significantly different due to the existence of LA. The first 7 days during degradation, the crystalline and amorphous regions of the fibrillar and lamellar crystals degraded together. The amorphous regions of fibrillar and lamellar crystals were basically degraded in 7–14 days, and then the crystalline regions began to accelerate degradation. In addition, the relative scattering intensity decreased at a slower rate with the increase of the heat-setting temperature, which also indicated that the degradation rate decreased with the heat-setting temperature. However, according to the scattering intensity, we have only discussed roughly the degradation period of the crystalline and amorphous regions in the fibrillar and lamellar crystals; certainly, a more detailed explanation of the scattering intensity needed to be combined with the mechanical properties, weight loss results, WAXD and SAXS data, which will be further discussed later in the degradation mechanism.

3.4. Degradation Mechanism. On the basis of the above results, the structural changes of PGA and P(GA-co-LA) during degradation could be roughly divided into four stages. A general schematic diagram of these changes during degradation is displayed in Figure 11. It was important to emphasize that the PGA and P(GA-co-LA) fibers used in experiments were mainly composed of fibrillar crystals with a small amount of lamellar crystals. In stage I (1–3 days of degradation), the preferential hydrolytic degradation occurred in the amorphous regions of polymer chains. The amorphous regions of the

fibrillar crystals of the PGA samples began to degrade partially, while the amorphous regions of the lamellar crystals were degraded almost completely, which corresponded to the increase of the scattering intensity of the fibrillar and lamellar crystals in Figure 10a,b. Certainly, the increase of the scattering intensity during the first day of the fibrillar crystals was larger than the changing trend of the scattering intensity of the lamellae, which indicated that the degradation might first occur in the amorphous regions of the fibrillar crystals. This corresponded to the fact that degradation first occurred at the surface, opening a channel, and then began to degrade the amorphous regions of the lamellar crystals. Nevertheless, we also tried to explain the location where degradation first occurred from the perspective of morphological changes. But because this change was so small that we did not see it even though we took SEM images. In stage II (3–7 days of degradation), part of the crystalline regions of the lamellar crystals began to degrade, corresponding to the gradual decrease of the lamellar scattering intensity; the amorphous regions of the fibrillar crystals were basically degraded in this stage. However, the degradation rate of lamellar crystals was significantly faster than fibrillar crystals, resulting in a slight increase in the degree of crystal orientation at this stage (Figure 5a). The corresponding increase in crystallinity at this stage was mainly attributed to the preferential degradation of amorphous chains (Figure 6a). The crystallite sizes of L_{110} and L_{020} were slightly increased (Figure 7c), whereas the unit cell parameters exhibited almost a constant value during this period (Figure 7a). Meanwhile, the degradation rate of the PGA fibers increased after some degraded oligomers were formed and trapped inside the sample, which autocatalyzed the degradation reaction with acidic end groups. Although very little mass of the PGA samples was lost during these two stages (Figure 2a), massive degradation of amorphous regions resulted in a substantial decrease in mechanical properties (Figure 1a). In stage III (7–14 days of degradation), as the molecular weight of the PGA fibers fell below a critical value, the degraded oligomers became soluble in water, and a large mass loss was observed. The mechanical properties can also be further reduced upon further degradation. Furthermore, the partial

degradation of the crystalline regions of the fibrillar crystals corresponded to the decrease of the scattering intensity, whereas the accelerated degradation of the crystalline regions of the lamellar crystals corresponded to the rapid decrease of the scattering intensity (Figure 10a,b). However, the obvious cleavage-induced crystallization, which usually formed defective crystals lamellae with smaller sizes, occurred in this stage. The apparent crystallite sizes L_{110} and L_{020} exhibited a gradual increase (Figure 7c), whereas the long period L and lamellar thickness L_c were found to decrease obviously due to the occurrence of cleavage-induced crystallization, which was probably because the confined spatial restrictions and lower molecular mass species would reduce the resultant lamellar thickness, causing the average long period and lamellar thickness to decrease, as presented in Figure 9a (covering both stages II and III). Originally, cleavage-induced crystallization would lead to a rapid increase in crystallinity, but due to the accelerated degradation of the crystalline regions at this stage, a large part of the molecular chains were trapped inside the sample after degradation; consequently, the crystallinity still showed a downward trend on the curve (Figure 6a). In stage IV (14–28 days of degradation), the crystalline regions of the lamellar crystals were basically degraded, and the scattering intensity was gradually reduced to 0 (Figure 10a), and most of the crystalline regions of the fibrillar crystal were also degraded. The further degradation of the crystalline regions resulted in a further decrease in crystallinity, as shown in Figure 6a. However, during the last stage of degradation, part of the skeleton of fiber samples began to collapse but still retained the original skeleton, which led to a slight decrease of orientation but still maintained a relatively large value (Figure 5a).

It was worth mentioning that the introduction of a part of LA units into the PGA skeleton reduced the degradation rate, leading to a degradation mechanism a little different from that of the PGA fiber. Although the degradation of P(GA-co-LA) fiber can also be roughly divided into four stages, unlike PGA, the degradation rate of P(GA-co-LA) fiber in the crystalline and amorphous regions was not so different during degradation. Since the initial crystallinity of P(GA-co-LA) fiber was smaller compared with PGA, the proportion of the amorphous regions was larger. In stage I (within 7 days of degradation), both the amorphous and crystalline regions of the fibrillar and lamellar crystals were degraded together, and the increase in the scattering intensity caused by the degradation of the amorphous regions was basically offset by the decrease in the scattering intensity caused by the degradation of the crystalline regions; therefore, the scattering intensity was basically unchanged or slightly increased, as shown in Figure 10c,d. Of course, the degradation rate of lamellar crystals was slightly faster than fibrillar crystals, resulting in an upward trend on the orientation curve (Figure 5b). In addition, the amorphous regions degraded at a faster rate than the crystalline regions, contributing to the increase of crystallinity within 7 days of degradation. In stage II (7–14 days of degradation), the amorphous regions of the fibrillar and lamellar crystals were basically degraded, and the crystalline regions were partially degraded. Very little mass of the P(GA-co-LA) samples was lost during these two stages (Figure 2b), but the mechanical properties began to decline significantly as a result of the degradation of amorphous regions. In stage III (14–21 days of degradation), the crystalline regions of fibrillar and lamellar crystals were degraded significantly, leading to a

decrease in the crystallinity. However, the obvious cleavage-induced crystallization phenomenon began to occur at this stage, resulting in an obvious decrease in a long period and lamellar thickness (Figure 9b). Moreover, it was found that the crystallinity of P(GA-co-LA) remained nearly constant at this stage; a reasonable interpretation was that the increase in crystallinity caused by cleavage-induced crystallization was in equilibrium with the decrease in crystallinity caused by accelerated degradation of crystalline regions. In the last stage of degradation (after 21 days of degradation), the crystalline regions of the fibrillar and lamellar crystals accelerated degradation, resulting in a rapid decrease in crystallinity (Figure 6b). Like PGA, some fiber skeleton collapse would occur during the degradation process; therefore, the orientation would decrease slightly in the later degradation period (Figure 5b). However, compared with PGA, the changing trend of orientation was obviously slower, which was due to the slower degradation rate.

In summary, combined with WAXD/SAXS data, weight loss, and mechanical property results, the degradation process of PGA and P(GA-co-LA) fibers was divided into four stages. The increase of crystallinity during the early stage of degradation and then a gradual decrease during the later period, indicating that preferential hydrolytic degradation occurred in the amorphous regions, followed by a further degradation in the crystalline regions. This was consistent with the results of previous studies on the degradation of PGA and P(GA-co-LA) fibers.^{25–28} It was worth mentioning that the current studies on the in vitro degradation of PGA and P(GA-co-LA) fibers had only given the specific mechanism of cleavage-induced crystallization, while structural changes during degradation were rarely analyzed in the previous literature studies. Based on the WAXD/SAXS data, the structural changes of PGA and P(GA-co-LA) fibers in different degradation stages were systematically presented in this study through the different degradation rates of fibrillar and lamellar crystals during degradation, and then the degradation mechanism was proposed in detail. It is most helpful for the preparation of the PGA and P(GA-co-LA) fibers with high performance.

4. CONCLUSIONS

The structural changes in PGA and P(GA-co-LA) fibers with different heat-setting temperatures during in vitro degradation were investigated by WAXD/SAXS, weight loss, and mechanical property tests. The results indicated that the degradation rate of PGA and P(GA-co-LA) fibers decreased with the heat-setting temperature, and the PGA fiber was more susceptible to the degradation process than P(GA-co-LA) fiber. The changing trend of crystallinity indicated that degradation occurred preferentially in the amorphous regions and then in the crystalline regions. The unit cell parameters showed a slight decrease, whereas the crystallite sizes showed a gradual increase during degradation. A schematic diagram of a four-stage model of the in vitro degradation mechanism was proposed through the different degradation rates of fibrillar and lamellar crystals during degradation. Very little mass of the PGA and P(GA-co-LA) samples was lost during the first two stages of degradation, while the mechanical properties showed a significant decline as a result of the rapid degradation of amorphous regions. The cleavage-induced crystallization process mainly occurred during stage III, contributing to the obvious decrease in the long period and lamellar thickness of both PGA and P(GA-co-LA) samples. In stage IV, the further

degradation of crystalline regions led to the further decrease of crystallinity. However, although the degradation process of PGA and P(GA-co-LA) fibers exhibited a similar four stages, the introduction of LA units significantly reduced the difference in the degradation rate of the amorphous and the crystalline regions so that the amorphous and crystalline regions of fibrillar and lamellar crystals were simultaneously degraded in the early stage of degradation, which ultimately led to the degradation mechanism of P(GA-co-LA) different from the PGA fibers. This research was not only important to understand the structural changes of PGA and P(GA-co-LA) fibers during degradation but also expected that the degradation mechanism obtained in this research could provide a theoretical basis for the preparation of the fibers with high performance.

■ ASSOCIATED CONTENT

SI Supporting Information

The Supporting Information is available free of charge at <https://pubs.acs.org/doi/10.1021/acsomega.1c04974>.

pH value changes of (a) PGA and (b) P(GA-co-LA) fibers during in vitro degradation with different heat-setting temperatures; 1D WAXD curves of PGA and P(GA-co-LA) fibers with the heat-setting temperature of 100 °C (a, c) and 140 °C (b, d) during in vitro degradation; 2D WAXD patterns of PGA fibers when (a) inclined (b) uninclined during degradation; changes in the crystallinity calculated from DSC results for (a) PGA and (b) P(GA-co-LA) samples with different heat-setting temperatures during degradation; and 1D SAXS curves of PGA and P(GA-co-LA) fibers with different heat-setting temperatures during degradation (PDF)

■ AUTHOR INFORMATION

Corresponding Author

Zongbao Wang – Ningbo Key Laboratory of Specialty Polymers, School of Materials Science and Chemical Engineering, Ningbo University, Ningbo 315211, China; orcid.org/0000-0002-7399-4638; Email: wangzongbao@nbu.edu.cn

Authors

Yushuang Miao – Ningbo Key Laboratory of Specialty Polymers, School of Materials Science and Chemical Engineering, Ningbo University, Ningbo 315211, China
Huashuai Cui – China Textile Academy, Beijing 100025, China
Zhimin Dong – Ningbo Key Laboratory of Specialty Polymers, School of Materials Science and Chemical Engineering, Ningbo University, Ningbo 315211, China
Yi Ouyang – Department of Radiation Oncology & State Key Laboratory of Oncology in South China, Sun Yat-sen University Cancer Center, Guangzhou 510060, China
Yiguo Li – Ningbo Key Laboratory of Specialty Polymers, School of Materials Science and Chemical Engineering, Ningbo University, Ningbo 315211, China; orcid.org/0000-0001-6620-2041
Qing Huang – China Textile Academy, Beijing 100025, China

Complete contact information is available at: <https://pubs.acs.org/doi/10.1021/acsomega.1c04974>

Author Contributions

[†]Y.M. and H.C. contributed equally to this work.

Notes

The authors declare no competing financial interest.

■ ACKNOWLEDGMENTS

This work was supported by the National Natural Science Foundation of China (51973097, 51773101). We thank Shanghai Synchrotron Radiation Facility (SSRF) for supporting the SAXS and WAXD tests.

■ REFERENCES

- (1) Jain, R. A. The manufacturing techniques of various drug loaded biodegradable poly(lactide-co-glycolide) (PLGA) devices. *Biomaterials* **2000**, *21*, 2475–2490.
- (2) Simon, C. G.; Khatri, C. A.; Wight, S. A.; Wang, F. W. Preliminary report on the biocompatibility of a moldable, resorbable, composite bone graft consisting of calcium phosphate cement and poly(lactide-co-glycolide) microspheres. *J. Orthop. Res.* **2002**, *20*, 473–482.
- (3) Karp, J.; et al. Bone formation on two-dimensional poly(DL-lactide-co-glycolide) (PLGA) films and three-dimensional PLGA tissue engineering scaffolds in vitro. *J. Biomed. Mater. Res.* **2003**, *64A*, 388–396.
- (4) Ouchi, T.; Ohya, Y. Design of lactide copolymers as biomaterials. *J. Polym. Sci., Part A: Polym. Chem.* **2004**, *42*, 453–462.
- (5) Jiang, W.; Gupta, R. K.; Deshpande, M. C.; Schwendeman, S. P. Biodegradable poly(lactic-co-glycolic acid) microparticles for injectable delivery of vaccine antigens. *Adv. Drug Delivery Rev.* **2005**, *57*, 391–410.
- (6) Ming, Z.; Zheng, Q.; Wang, J.; Wang, Y.; Hao, J. The Construction and Investigation of PLGA Artificial Bone by Biomimetic Mineralization. *J. Huazhong Univ. Sci. Technol., Med. Sci.* **2005**, *25*, 687.
- (7) Wen, X.; Tresco, P. A. Fabrication and characterization of permeable degradable poly(DL-lactide-co-glycolide) (PLGA) hollow fiber phase inversion membranes for use as nerve tract guidance channels. *Biomaterials* **2006**, *27*, 3800–3809.
- (8) Navarro, M.; Aparicio, C.; Charles-Harris, M.; Ginebra, M. P.; Engel, E.; Planell, J. A. Development of a Biodegradable Composite Scaffold for Bone Tissue Engineering: Physicochemical, Topographical, Mechanical, Degradation, and Biological Properties. *Adv. Polym. Sci.* **2006**, *200*, 209–231.
- (9) Chang, C. J.; Hsu, S. H. The effect of high outflow permeability in asymmetric poly(DL-lactic acid-co-glycolic acid) conduits for peripheral nerve regeneration. *Biomaterials* **2006**, *27*, 1035–1042.
- (10) Venkatraman, S. S.; Tan, L. P.; Joso, J.; Yin, C.; Wang, X. Biodegradable stents with elastic memory. *Biomaterials* **2006**, *27*, 1573–1578.
- (11) Cao, Y.; Mitchell, G.; Messina, A.; Price, L.; Thompson, E.; Penington, A.; Morrison, W.; O'Connor, A.; Stevens, G.; Cooper-White, J. The influence of architecture on degradation and tissue ingrowth into three-dimensional poly(lactic-co-glycolic acid) scaffolds in vitro and in vivo. *Biomaterials* **2006**, *27*, 2854–2864.
- (12) Mehta, A. K.; Khushwant, S. Y.; Krutika, K. S. Nimodipine Loaded PLGA Nanoparticles: Formulation Optimization Using Factorial Design, Characterization and In Vitro Evaluation. *Curr. Drug Delivery* **2007**, *4*, 185–193.
- (13) Charles-Harris, M.; Valle, S. D.; Hentges, E.; Bleuet, P.; Lacroix, D.; Planell, J. A. Mechanical and structural characterisation of completely degradable poly(lactic acid/calcium phosphate glass scaffolds. *Biomaterials* **2007**, *28*, 4429–4438.
- (14) Therin, M.; Pascal, C.; Suming, L.; Henri, et al. In vivo degradation of massive poly(α -hydroxy acids): Validation of In vitro findings. *Biomaterials* **1992**, *13*, 594–600.
- (15) Miller, R. A.; Brady, J. M.; Cutright, D. E. Degradation rates of oral resorbable implants (poly(lactates and polyglycolates): Rate

modification with changes in PLA/PGA copolymer ratios. *J. Biomed. Mater. Res.* **1977**, *11*, 711–719.

(16) Nakamura, T.; Hitomi, S.; Watanabe, S. J.; Shimizu, Y.; Ikada, Y.; et al. Bioabsorption of polylactides with different molecular properties. *J. Biomed. Mater. Res.* **1989**, *23*, 1115–1130.

(17) Martin, O.; Avérous, L. Poly(lactic acid): plasticization and properties of biodegradable multiphase systems. *Polymer* **2001**, *42*, 6209–6219.

(18) Fu, B. X.; Hsiao, B. S.; Chen, G.; Zhou, J.; Koyfman, I.; Jamiolkowski, D.; Dormier, E. Structure and property studies of bioabsorbable poly(glycolide-co-lactide) fiber during processing and in vitro degradation. *Polymer* **2002**, *43*, 5527–5534.

(19) M Ac Donald, R. T.; Mccarthy, S. P.; Gross, R. A. Enzymatic Degradability of Poly(lactide): Effects of Chain Stereochemistry and Material Crystallinity. *Macromolecules* **1996**, *29*, 7356–7361.

(20) Park, A.; Cima, L. G. In vitro cell response to differences in poly-L-lactide crystallinity. *J. Biomed. Mater. Res.* **2007**, *31*, 117–130.

(21) Schugens, C.; Maquet, V.; Grandfils, C.; Jerome, R.; Teyssie, P. Polylactide macroporous biodegradable implants for cell transplantation. II. Preparation of polylactide foams by liquid-liquid phase separation. *J. Biomed. Mater. Res., Part A* **1996**, *30*, 449–461.

(22) Cordewener, F. W.; Rozema, F. R.; Bos, R.; Boering, G. Material properties and tissue reaction during degradation of poly(96L/4D-lactide)-a study in vitro and in rats. *J. Mater. Sci.: Mater. Med.* **1995**, *6*, 211–217.

(23) Chu, C. C. Hydrolytic degradation of polyglycolic acid: Tensile strength and crystallinity study. *J. Appl. Polym. Sci.* **1981**, *26*, 1727–1734.

(24) Izumikawa, S.; Yoshioka, S.; Aso, Y.; Takeda, Y. Preparation of poly(L-lactide) microspheres of different crystalline morphology and effect of crystalline morphology on drug release rate. *J. Controlled Release* **1991**, *15*, 133–140.

(25) Chu, C. C. An in-vitro study of the effect of buffer on the degradation of poly(glycolic acid) sutures. *J. Biomed. Mater. Res.* **1981**, *15*, 19–28.

(26) Chu, C. C. Hydrolytic degradation of polyglycolic acid: Tensile strength and crystallinity study. *J. Appl. Polym. Sci.* **2010**, *26*, 1727–1734.

(27) Fredericks, R. J.; Melveger, A. J.; Dolegiewitz, L. J. Morphological and structural changes in a copolymer of glycolide and lactide occurring as a result of hydrolysis. *J. Polym. Sci., Polym. Phys. Ed.* **1984**, *22*, 57–66.

(28) King, E.; Cameron, R. E. Effect of hydrolytic degradation on the microstructure of poly(glycolic acid): An X-ray scattering and ultraviolet spectrophotometry study of wet samples ultraviolet. *J. Appl. Polym. Sci.* **1997**, *66*, 1681–1690.

(29) Fu, B. X. A study of structure and property changes of biodegradable polyglycolide and poly(glycolide-co-lactide) fibers during processing and in vitro degradation. *Chin. J. Polym. Sci.* **2003**, *21*, 159–167.

(30) Li, S. Hydrolytic degradation characteristics of aliphatic polyesters derived from lactic and glycolic acids. *J. Biomed. Mater. Res.* **1999**, *48*, 342–350.

(31) Zong, X.-H.; Wang, Z. G.; Hsiao, B. S.; Chu, B.; et al. Structure and Morphology Changes in Absorbable Poly(glycolide) and Poly(glycolide-co-lactide) during in Vitro Degradation. *Macromolecules* **1999**, *32*, 8107–8114.

(32) Dong, Z.; Miao, Y.; Cui, H.; Huang, Q.; Li, Y.; Wang, Z. Structural evolution of polyglycolide and poly(glycolide-co-lactide) fibers during heat-setting. *Biomacromolecules* **2021**, *22*, 3342–3356.

(33) Vert, M.; Li, S. M.; Spenlehauer, G.; Guerin, P. J. Bioresorbability and Biocompatibility of Aliphatic Polyesters. *J. Mater. Sci.: Mater. Med.* **1992**, *3*, 432–446.

(34) Li, X. ipyChord: a package for evaluating small-angle X-ray scattering data of fiber symmetry. *J. Appl. Crystallogr.* **2021**, *54*, 680–685.

(35) Li, S. M.; Vert, M. Biodegradation of Aliphatic Polyesters. In *Degradable Polymers*, 2002; Vol. 4, pp 123–135.

(36) Hammersley, A. P.; Svensson, S. O.; Thompson, A. Calibration and correction of spatial distortions in 2D detector systems. *Nucl. Instrum. Methods Phys. Res., Sect. A* **1994**, *346*, 312–321.

(37) Alexander, L. E. X-ray diffraction methods in polymer science. *J. Mater. Sci.* **1971**, *6*, 93.

(38) Kortleve, G.; Vonk, C. G. X-ray small-angle scattering of bulk polyethylene. *Kolloid-Z. Z. Polym.* **1968**, *225*, 124–131.

(39) Montes de Oca, H.; Farrar, D. F.; Ward, I. M. Degradation studies on highly oriented poly(glycolic acid) fibres with different lamellar structures. *Acta Biomater.* **2011**, *7*, 1535–1541.

(40) Vonk, C. G. Investigation of non-ideal 2-phase polymer structures by small-angle X-ray-scattering. *J. Appl. Crystallogr.* **1973**, *6*, 81–86.

(41) Strobl, G. R.; Schneider, M. J. Direct evaluation of the electron density correlation function of partially crystalline polymers. *J. Polym. Sci., Part A: Polym. Chem.* **2010**, *18*, 1343–1359.

(42) Schmitt, E. A.; Flanagan, D. R.; Linhardt, R. J. Importance of distinct water environments in the hydrolysis of poly(DL-lactide-co-glycolide). *Macromolecules* **1994**, *27*, 743–748.

(43) Liu, Y.; Bai, X.; Liang, A. Synthesis, Properties, and In Vitro Hydrolytic Degradation of Poly(d,l-lactide-co-glycolide-co-ε-caprolactone). *Int. J. Polym. Sci.* **2016**, *2*, 1–9.

(44) King, E.; Cameron, R. E. Effect of hydrolytic degradation on the microstructure of poly(glycolic acid): An X-ray scattering and ultraviolet spectrophotometry study of wet samples ultraviolet. *J. Appl. Polym. Sci.* **1997**, *66*, 1681–1690.

(45) Lostocco, M. R.; Murphy, C. A.; Cameron, J. A.; Huang, S. J. The effects of primary structure on the degradation of poly(ε-caprolactone)/poly(L-lactide) block copolymers. *Polym. Degrad. Stab.* **1998**, *59*, 303–307.

(46) Hurrell, S.; Cameron, R. E. The effect of initial polymer morphology on the degradation and drug release from polyglycolide. *Biomaterials* **2002**, *23*, 2401–2409.

(47) You, Y.; Min, B. M.; Lee, S. J.; Lee, T. S.; Park, W. H. In vitro degradation behavior of electrospun polyglycolide, polylactide, and poly(lactide-co-glycolide). *J. Appl. Polym. Sci.* **2005**, *95*, 193–200.

(48) Sato, H.; Miyada, M.; Yamamoto, S.; Raghunatha Reddy, K.; Ozaki, Y. C–HO (ether) hydrogen bonding along the (110) direction in polyglycolic acid studied by infrared spectroscopy, wide-angle X-ray diffraction, quantum chemical calculations and natural bond orbital calculations. *RSC Adv.* **2016**, *6*, 16817–16823.

(49) Wang, Z.-G.; Hsiao, B. S.; Zong, X. H.; Yeh, F.; Zhou, J. J.; Dormier, E.; Jamiolkowski, D. D. Morphological development in absorbable poly(glycolide), poly(glycolide-co-lactide) and poly(glycolide-co-caprolactone) copolymers during isothermal crystallization. *Polymer* **2000**, *41*, 621–628.

(50) Guruswamy, K.; Verma, R. K.; Kornfield, J. A.; Yeh, F.; Hsiao, B. S. Shear Induced Crystallization in Isotactic Polypropylene: Optical and SAXS Studies. *Am. Phys. Soc.* **1998**, *5*, 23–35.

(51) Hsiao, B. S.; Sauer, B. B.; Verma, R. K.; Zachmann, G.; et al. New Insight of Isothermal Melt Crystallization in Poly(aryl ether ketone) via Time-Resolved Simultaneous Small-Angle X-ray Scattering/Wide-Angle X-ray Diffraction Measurements. *Macromolecules* **1995**, *28*, 6931–6936.